The morphology of amorphous SiO_2 surfaces during low energy ion sputtering

2009 J. Phys.: Condens. Matter 21 495305

(http://iopscience.iop.org/0953-8984/21/49/495305)

J. Phys.: Condens. Matter **21** (2009) 495305 (7pp) doi:10.1088/0953-8984/21/49/495305

The morphology of amorphous SiO_2 surfaces during low energy ion sputtering

Adrian Keller[1], **Stefan Facsko and Wolfhard Möller**

Institute of Ion Beam Physics and Materials Research, Forschungszentrum Dresden-Rossendorf, PO Box 510119, 01314 Dresden, Germany

E-mail: adrian@inano.au.dk

Received 27 August 2009, in final form 21 October 2009
Published 13 November 2009
Online at stacks.iop.org/JPhysCM/21/495305

Abstract

The morphology of different amorphous or amorphized SiO_2 surfaces, including thermally grown films, fused silica, and single crystalline quartz, during low energy ion sputtering has been investigated by means of atomic force microscopy. For all three materials, the formation of periodic ripple patterns oriented normal to the direction of the ion beam is observed at intermediate incident angles. At near-normal incidence, the SiO_2 surfaces remain flat, whereas a rotation of the ripple patterns is observed at grazing incidence. At intermediate angles, the patterns on the different surfaces exhibit wavelength coarsening of different strengths, which can be attributed to different amounts of near-surface mass transport by the surface-confined ion-enhanced viscous flow. In the framework of the recent hydrodynamic model of ion erosion, the observed differences in ripple coarsening are consistent with this interpretation and indicate that the surface energies of thermally grown SiO_2 and amorphized quartz are lower and higher than that of fused silica, respectively.

(Some figures in this article are in colour only in the electronic version)

1. Introduction

The ion-induced formation of surface nanopatterns is a topic of intense experimental [1] and theoretical [2] research. These regular patterns form spontaneously by self-organization during low and medium energy ion sputtering on the eroded surface. Depending on the irradiation conditions, different pattern types can be fabricated. For oblique ion incidence, ordered ripple patterns have been observed [3] whereas normal incidence ion sputtering leads to the formation of hexagonally ordered dot patterns [4]. Such patterns have been found on the surfaces of different amorphous and crystalline materials including insulators [5], semiconductors [3], and metals [6, 7]. The periodicity of the patterns is determined by the experimental conditions and ranges from less than twenty nanometers [8] up to more than one micron [9].

The formation of regular patterns during ion sputtering has been explained in the Bradley–Harper (BH) model [10] which is based on Sigmund's theory of sputtering [11]. Sigmund showed that the local erosion rate at a given point of the surface is proportional to the total energy deposited in this point by the nuclear collision cascades of the ions impinging at all points of the surface. Then, in the case of a rough surface, the local erosion rate depends on the local curvature of the surface and is higher in depressions than on elevations [12]. Therefore, a rough surface is unstable under ion bombardment as its initial roughness spectrum gets amplified. In the presence of a competing smoothing mechanism like thermally activated surface diffusion, however, a wavelength selection is observed with one spatial frequency growing fastest [10].

The linear BH model predicts the formation of regular ripple patterns oriented normal and parallel to the direction of the ion beam at near-normal and grazing ion incidence, respectively [10]. The amplitude of these ripples grows exponentially in time. However, in order to account for certain experimentally observed features of the pattern evolution in the limit of long sputter times, e.g. the saturation of the ripple amplitude [13] or the coarsening of the ripple wavelength [8], several nonlinear extensions of the BH equation have been subsequently proposed that also consider higher order terms [2, 14–16].

Although lots of research has been dedicated to the understanding of the underlying mechanisms of ion-induced pattern formation, the technological relevance of such patterns

[1] Present address: Interdisciplinary Nanoscience Center (iNANO), University of Aarhus, DK-8000 Aarhus, Denmark.

was recognized only during the last few years. In recent experiments, the principal applicability of ion-induced nanopatterns in microelectronic device fabrication [17] as well as in the creation of novel magnetic storage media [18] has been demonstrated. In addition, rippled surfaces are of interest as prepatterned templates in the growth of thin metallic films. These films were found to exhibit additional optical [19, 20] and magnetic [21, 22] anisotropies when grown on nanorippled substrates. Especially nanorippled SiO_2 surfaces are of growing relevance, e.g. for optical applications [20] or as diffusion barriers in the fabrication of metallic nanoparticle and nanowire arrays [23]. For these applications, the precise control of the pattern properties is a crucial task. However, the few experimental studies [5, 24, 25] of the ripple formation and evolution on SiO_2 surfaces yield partially contradictory results as, e.g., coarsening of the ripple wavelength was observed during ion sputtering of fused silica surfaces [25] but not on thermally grown SiO_2 films [24]. These differences in the evolution of the ripple patterns can be attributed to the different nature of the SiO_2 substrates [26]. In this paper, we extend our previous study [26] on the formation and evolution of ion-induced ripple patterns during low energy ion sputtering of different amorphous or amorphized SiO_2 surfaces. We show that thermally grown SiO_2 films, fused silica, and amorphized quartz surfaces exhibit similar dependencies of the ripple patterns on the incident angle and the ion energy but different wavelength coarsening. Furthermore, we show that in the framework of the hydrodynamic model of ion erosion [16], a nonlinear generalization of the linear BH equation, the observed differences in the coarsening of the ripple patterns on the different surfaces are consistent with differences in the surface smoothing by surface-confined ion-enhanced viscous flow as induced by different surface energies. From the comparison with the hydrodynamic model, the surface energies of thermally grown SiO_2 and amorphized quartz can be estimated to be lower and higher than that of fused silica, respectively.

2. Experimental details

The experiments of this work have been carried out at room temperature in a high vacuum chamber with a base pressure of $\sim 10^{-8}$ mbar. A Kaufman type ion source has been used for the sputtering, providing a broad beam of Ar^+ ions with a constant flux of 1.2×10^{15} cm^{-2} s^{-1}. The ion energy was $\leqslant$1000 eV and the applied fluence ranged from 1×10^{17} to 1.5×10^{18} cm^{-2}. In order to avoid charging of the sample surfaces during the sputtering a hot filament has been placed above the sample in a distance of about 10 cm. After the irradiation, the sample surfaces have been examined by atomic force microscopy (AFM).

The samples processed in these experiments were thermally grown SiO_2 films, fused silica, and single crystalline quartz. The thermal SiO_2 films were grown by wet oxidation of Si(001) surfaces. The films had a nominal thickness of 1.5 μm and a root mean square (rms) surface roughness of $w_g \sim 0.5$ nm. The fused silica samples were commercially available polished SUPRASIL® wafers with $w_f \sim 0.7$ nm. The quartz samples were polished (0001) oriented wafers with $w_q \sim 0.3$ nm. Due to the impact of the impinging ions, the crystalline SiO_2(0001) surface is amorphized during the irradiation resulting in a thin amorphous top layer. At the fluences of $\geqslant 1 \times 10^{17}$ cm^{-2} applied in the current experiments the quartz surface should be fully amorphous as has been confirmed by TRIM [27] calculations [26].

AFM measurements have been performed in air using a MultiMode™ scanning probe microscope with a NanoScope IV controller from Veeco Instruments in tapping mode. 2×2 μm^2 images with 1024 points per scan line were usually taken. PointProbe® Plus tips (PPP-NCLR) for non-contact and tapping mode operation from NANOSENSORS™ have been used. The tip apex has a radius typically smaller than 7 nm and a half cone angle of less then 10°. The ripple wavelengths have been determined from the two-dimensional Fourier transforms of the AFM images and are in good agreement with those determined from complementary imaging techniques in real and reciprocal space such as transmission electron microscopy and grazing incidence x-ray scattering (not shown).

3. Results

Figure 1 shows AFM images of the surfaces of the three SiO_2 materials before and after sputtering with 500 eV ions at a fluence of $\Phi = 1 \times 10^{18}$ cm^{-2} and different incident angles. For all three SiO_2 states, similar dependencies of the surface morphology on the incident angle are observed. At rather low incident angles ($\theta = 30°$, second row of figure 1), the surfaces remain flat but exhibit a slightly reduced surface roughness as can be seen in figure 2 which shows the dependence of the rms surface roughness on the angle of incidence. This indicates a smoothing of the SiO_2 surfaces at such low incident angles.

At larger incident angles $\theta \geqslant 45°$ (third row of figure 1), the surfaces develop ripple patterns that are oriented normal to the direction of the ion beam. Here, certain differences between the morphologies of the different SiO_2 surfaces become apparent. In the case of the thermally grown (figure 1(g)) and the fused (figure 1(h)) silica surfaces, the general surface morphologies and also the ripple wavelengths are similar with $\lambda_{g,f} \sim 30$ nm. The morphology of the amorphized quartz surface (figure 1(i)), however, appears certainly different from the fused and the grown silica surfaces. Here, the wavelength of the observed ripple pattern is smaller with $\lambda_q \sim 22$ nm. In addition, the patterns on quartz are not as well pronounced as the patterns on thermally grown and fused silica what is reflected in the lower surface roughness (see figure 2).

At grazing ion incidence (fourth row of figure 1, $\theta = 72°$), very different morphologies are observed. Here, no well ordered ripple patterns are found anymore and the surfaces in all three cases exhibit a well pronounced (cf figure 2) morphology consisting of quasi-periodic structures that are elongated along the beam direction. In all three cases, the periodicity of these structures is about 100 nm. Similar structures have already been observed in previous grazing incidence experiments on SiO_2 surfaces [25].

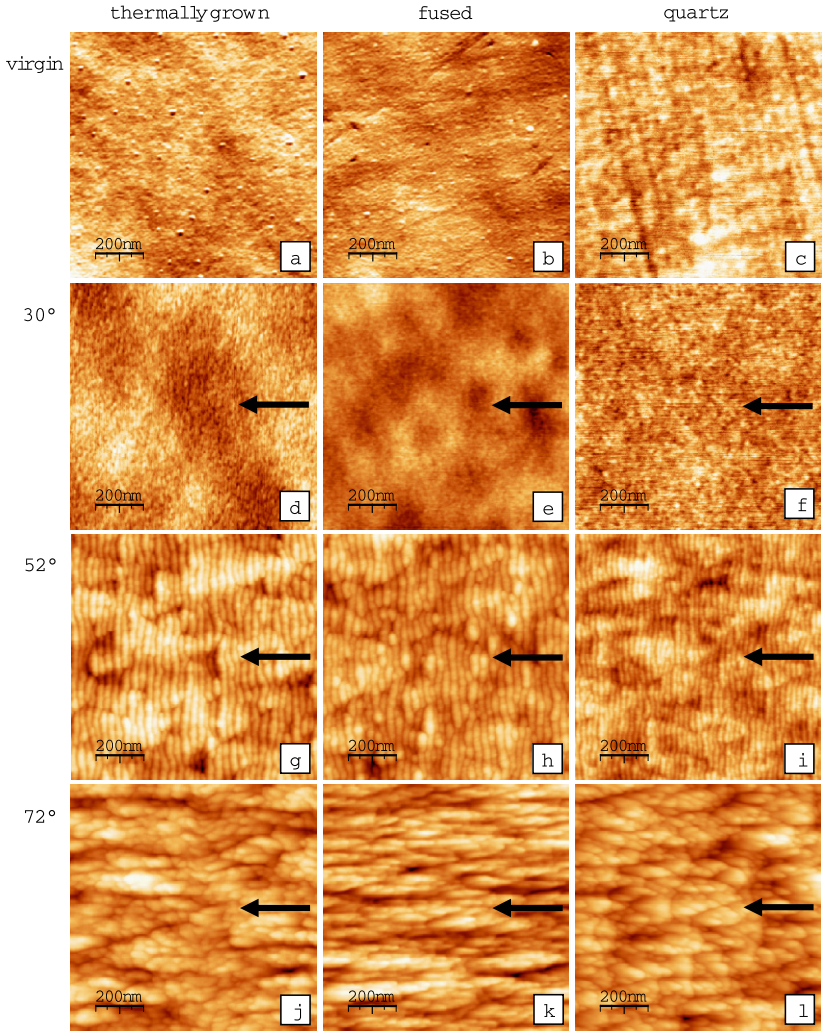

Figure 1. Surface morphology of thermally grown SiO_2 (left), fused silica (center), and quartz (right) after sputtering with 500 eV at an incident angle $\theta = 30°$ (second row), 52° (third row), and 72° (fourth row) with respect to the surface normal. The applied fluence was $\Phi = 1 \times 10^{18}$ cm^{-2}. The first row depicts AFM images of the virgin substrates. The height scales are 3 nm (a), 6 nm (b), 1 nm (c), (f), 2 nm (d), 4 nm (e), 11 nm (g), 13 nm (h), 8 nm (i), 18 nm (j), (k), and 28 nm (l). The direction of the incident ion beam is indicated by the arrows.

The dependence of the morphology of the SiO_2 surfaces on the ion energy is shown in figure 3 which gives AFM images of the three SiO_2 surfaces after sputtering with an energy of 500 eV (first row) and 1000 eV (second row). In all three cases, the periodicity as well as the height of the ripples is increasing. The dependence of the ripple wavelength on the ion energy is shown in figure 4. In agreement with previous studies [24], the ripple wavelength on all three surfaces increases linearly with ion energy. However, different quantitative dependencies of the ripple wavelength on the ion energy are observed with fused silica and quartz exhibiting the strongest and weakest increase, respectively.

In order to investigate the coarsening of the ripple patterns on the different SiO_2 materials, the temporal evolution of the patterns has been studied. For this, several samples of each material have been sputtered with different fluences Φ in the range from 1×10^{17} to 1.5×10^{18} cm^{-2} at an incident angle $\theta = 52°$ and an energy of 500 eV. The resulting morphologies for two different fluences are shown in figure 5. Qualitatively

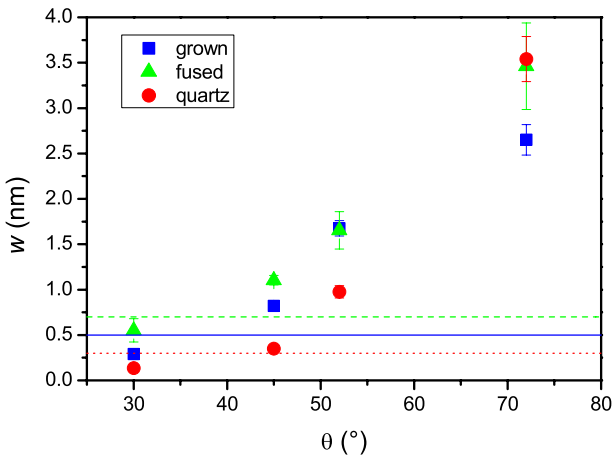

Figure 2. Dependence of the rms surface roughness w on the incident angle for sputtering with 500 eV Ar ions at an applied fluence of $\Phi = 1 \times 10^{18}$ cm^{-2}. The horizontal lines correspond to the roughness of the virgin substrates (solid line—thermally grown oxide, broken line—fused silica, dotted line—quartz).

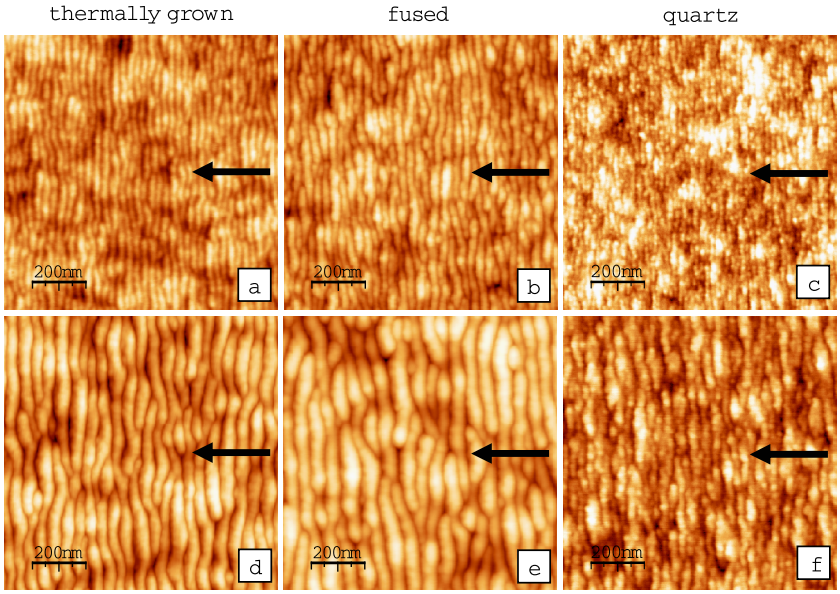

Figure 3. Surface morphology of thermally grown SiO_2 ((a), (d)), fused silica ((b), (e)), and quartz ((c), (f)) after sputtering under 45° incidence at an ion energy of 500 (first row) and 1000 eV (second row). The applied fluence was $\Phi = 1 \times 10^{18}$ cm^{-2}. The height scales are 6 nm (a), 8 nm (b), 2 nm (c), 13 nm (d), 15 nm (e), and 3 nm (f). The direction of the incident ion beam is indicated by the arrows.

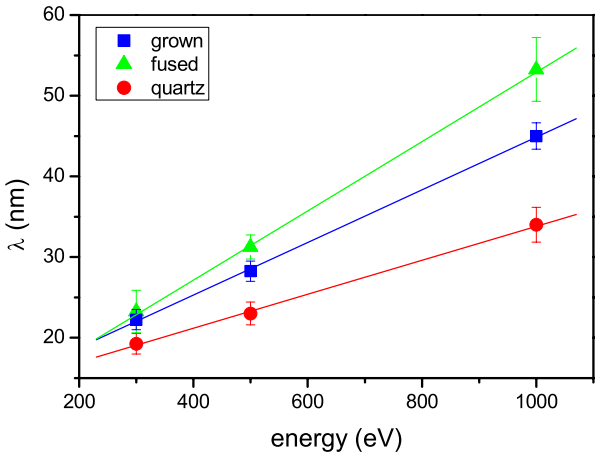

Figure 4. Dependence of the ripple wavelength λ on the ion energy. The applied fluence was $\Phi = 1 \times 10^{18}$ cm^{-2} at an incident angle of 45°. The straight lines are to guide the eye.

the fluence dependence of the surface morphology is rather similar for the three SiO_2 materials. At low fluences (first row of figure 5), the morphologies are dominated by rather well ordered ripple patterns. At higher fluences (second row of figure 5), the ripple patterns are superposed by kinetic roughening at larger length scales with the ripple patterns getting more disordered. However, the wavelength of the ripples on thermally grown SiO_2 (figures 5(a) and (d)) is increasing significantly with fluence in the depicted fluence range from 5×10^{17} to 1.5×10^{18} cm^{-2} whereas this effect is smaller on quartz.

For the three SiO_2 materials, figure 6 gives the evolution of the ripple wavelength λ as determined from the Fourier transforms of the AFM images. For the thermally grown SiO_2 films, the wavelength increases roughly linear with fluence. The initial and the final (though not necessarily saturated) wavelength is $\lambda_g \sim 22$ nm and $\lambda_g \sim 35$ nm, respectively. In the case of fused silica, however, a rather different dynamics is observed. Here, the ripple wavelength increases stronger in the beginning but saturates already at a fluence of $\Phi = 5 \times 10^{17}$ cm^{-2}. The values of the initial and the final wavelength are slightly higher and lower than for the grown films, respectively. A completely different situation is found for the amorphized quartz surface where the wavelength remains constant at $\lambda_q \sim 22$ nm and no ripple coarsening is found at all.

4. Discussion

The linear continuum equation derived by Bradley and Harper successfully describes the formation and early evolution of ion-induced ripple patterns and is given by [10]

$$\partial_t h = -v_0 + \beta \partial_x h + \nu_x \partial_x^2 h + \nu_y \partial_y^2 h - D\nabla^4 h \qquad (1)$$

with the surface height function $h(x, y, t)$. Here, the projected direction of the ion beam is parallel to the x axis. The first and second term on the rhs of equation (1) represent the erosion velocity v_0 and the lateral motion of the patterns with constant β, respectively, and do not influence the topography development. The third and the fourth term induce an instability of the surface in the x and y direction for negative ν_x and ν_y, respectively. In the fifth term, D represents the relaxation rate for diffusional surface smoothing.

With increasing angle of incidence, the BH equation predicts a rotation of the ripple pattern from normal to parallel with respect to the ion beam. In agreement with this prediction, a transition from ordered ripples oriented normal to the ion beam direction at intermediate angles to ripple-like structures oriented parallel to the beam at grazing angles was found on all

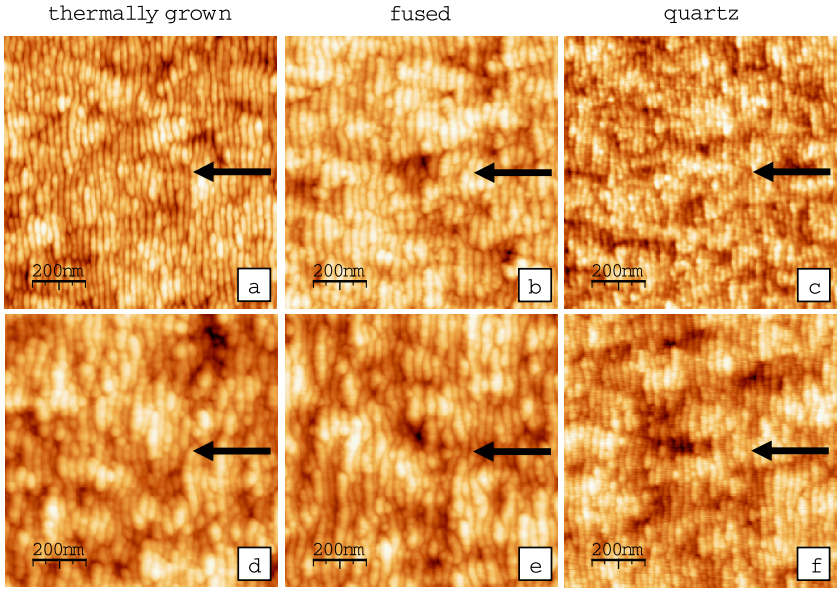

Figure 5. Surface morphology of thermally grown SiO_2 (left), fused silica (center), and quartz (right) after sputtering with 500 eV at an incident angle $\theta = 52°$. The applied fluence was $\Phi = 5 \times 10^{17}$ cm^{-2} (first row) and 1.5×10^{18} cm^{-2} (second row). The height scales are 7 nm (a), 14 nm ((b), (d)), 4 nm (c), 15 nm (e), 8 nm (f). The direction of the incident ion beam is indicated by the arrows.

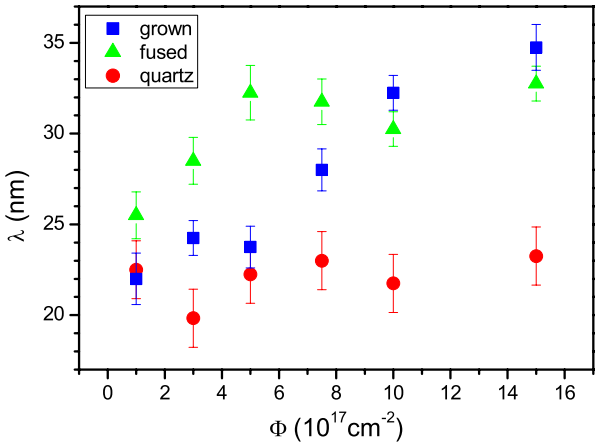

Figure 6. Evolution of the ripple wavelength λ versus fluence Φ for sputtering with 500 eV ions at 52° incidence.

three SiO_2 surfaces. However, as pointed out by Davidovitch *et al* [28], the observed smoothing of the sputtered surface at $\theta = 30°$ cannot be explained within the BH model and its nonlinear extensions. Carter and Vishnyakov explained a similar observation on Si surfaces bombarded with higher energy ions as caused by an additional ion-induced mass transport along the surface that acts mainly at normal and near-normal incidence but is of minor importance at larger incident angles [29]. This so-called ballistic diffusion can also be introduced into the BH equation where it results in an additional term proportional to $\nabla^2 h$ [29, 28]. A similar mechanism has also been proposed for lower ion energies [28].

In equation (1), the surface relaxation rate D might include different smoothing mechanisms like thermally activated surface self-diffusion (TSD) [10, 30], ion-induced surface diffusion (ISD) [31], and ion-enhanced viscous flow (IVF) in the case of amorphous or amorphized surfaces like silica [24]. These different smoothing mechanisms lead to different energy dependencies of the ripple wavelength [1]. For TSD being the main smoothing mechanism, the ripple wavelength is predicted to decrease with increasing ion energy. However, if either ISD or IVF dominate the smoothing, the wavelength will increase with ion energy. Thus, the observed increase of the ripple wavelength with ion energy (cf figure 4) indicates that TSD is only of minor importance and the surface smoothing is dominated by ISD or IVF.

If ISD dominates the smoothing of the surface with $D = D_{\mathrm{ISD}}$, equation (1) will include only erosive terms since ISD does not involve any surface mass transport and is of purely erosive nature [31]. In this case, all the coefficients in equation (1) will result from the series expansion of the Sigmund integral equation and thus only depend on the energy deposition in the surface by the impinging ion [10, 31]. However, it is rather unlikely that the energy deposition in the different substrate materials differs significantly enough in order to explain the observed differences [26]. Thus, above observations are probably caused by differences in the surface smoothing by IVF.

When bombarding amorphous surfaces with energetic ions, surface smoothing is significantly influenced by IVF [32]. In the case of low energy ion bombardment, however, this IVF is confined into a thin surface layer of thickness d which is of the order of the ion penetration depth a [24]. Then, $D = D_{\mathrm{IVF}} = d^3\gamma/\eta_{\mathrm{S}}$ with the surface energy γ and the surface viscosity η_{S}. For IVF being the main smoothing mechanism, the ripple wavelength again should increase with ion energy [24] in agreement with our experimental observations. Since $d \sim a$ should be similar for the different SiO_2 states under investigation, only differences in the surface energy γ and the surface viscosity η_{S} can be responsible for the

observed differences in the morphology evolution. Indeed, it has been shown both experimentally [5] and theoretically [33] that the surface energy of SiO_2 may vary strongly depending on the nature and history of the samples. For the viscosity of different SiO_2 surfaces, however, experimental data is scarce especially under low energy heavy-ion bombardment. Nevertheless, different surface smoothing rates due to surface-confined IVF can be expected for the different SiO_2 specimens due to differences in the surface energy γ.

Since equation (1) incorporates only linear terms, it is not able to reproduce nonlinear features of the surface evolution like the coarsening of the ripple wavelength. Up to now, the only nonlinear generalization of the BH equation that is able to show (interrupted) wavelength coarsening is the hydrodynamic model of ion erosion. This model was derived by Muñoz-García and coworkers [16, 34] by coupling of two height fields, namely the surface height function and the thickness of the mobile surface adatom layer, respectively. The resulting nonlinear continuum equation is given by [16]

$$\partial_t h = -v_0 + \beta\partial_x h + \sum_{i=x,y}\{\nu_i\partial_i^2 h + \zeta_i^{(1)}(\partial_i h)^2\} - \sum_{i,j=x,y}\{K_{ij}\partial_i^2\partial_j^2 h + \zeta_{ij}^{(2)}\partial_i^2(\partial_j h)^2\}. \quad (2)$$

Here, the terms proportional to $\zeta_{ij}^{(2)}$ and $\zeta_i^{(1)}$ are conserved and nonconserved Kardar–Parisi–Zhang (KPZ) [35] nonlinearities, respectively. In the frame of Sigmund's Gaussian approximation [12], the ν_i coefficients of equation (2) are proportional to the corresponding coefficients of equation (1) but also incorporate the redeposition of sputtered material [34] which should again be similar for the different SiO_2 materials. In a similar manner, the $\zeta_i^{(1)}$ coefficients depend only on the energy deposition in the surface and the amount of redeposited material, and should thus be constant for the different SiO_2 surfaces [34]. K_{ij} includes the relaxation rate D_{ISD} as well as smoothing due to TSD and IVF.

For constant ν_i and $\zeta_i^{(1)}$, the strength as well as the interruption of the ripple coarsening in the hydrodynamic model depends only on the smoothing rate $K_{ij} \propto D_{\mathrm{IVF}}$ and $\zeta_{ij}^{(2)}$ which again depend weakly on the relaxation rate D_{IVF} [34, 36]. Therefore, differences in the surface smoothing will result in different coarsening of the ripples. Comparing the different coarsening behaviors observed in the experiments, one finds that the ripple wavelength saturates earlier for fused silica than for the grown films (see figure 6). Neglecting the weak D_{IVF} dependence of $\zeta_{ij}^{(2)}$, this indicates that the value of K_{ij} and therefore also D_{IVF} is larger for fused than for grown silica [36, 34]. In this case, also the saturated ripple wavelength should be smaller for the higher D_{IVF} (i.e. for fused silica) what appears to be valid for our experimental data. The absence of coarsening on quartz surfaces indicates an even higher value of D_{IVF}. Thus, when neglecting possible contributions of the surface viscosity η_{S}, one would expect the surface energies of thermally grown SiO_2, γ_{g}, and amorphized quartz, γ_{q}, to be lower and higher than that of fused silica, γ_{f}, $\gamma_{\mathrm{g}} < \gamma_{\mathrm{f}} < \gamma_{\mathrm{q}}$. These different surface energies might result from different numbers of broken Si–O–Si bonds. It is known that the number of broken Si–O–Si bonds depends on the fabrication of the SiO_2 sample and has a strong influence on its surface energy [33].

In contrast to our observations, Umbach *et al* found nearly no wavelength coarsening during sputtering of thermally grown wet SiO_2 films [24]. Based on above analysis, this discrepancy indicates a higher surface energy of those oxide films which could result from different growth conditions (temperature, H_2O pressure, etc). In addition, the films used by Umbach *et al* had a thickness of only 500 nm and are thus thinner than the ones used in the present experiments what might also influence the surface energy.

5. Conclusion

In conclusion, we have investigated the formation and evolution of regular ripple patterns induced by low energy ion sputtering of different amorphous or amorphized SiO_2 surfaces, namely thermally grown SiO_2 films, fused silica, and single crystalline quartz. For all surfaces, a qualitatively similar dependence of the surface morphology on the incident angle is observed. At near-normal incidence, the surface is smoothed what can be explained by the importance of ballistic diffusion at small incident angles [29, 28]. In agreement with the BH model [10] and previous experimental studies [25], periodic ripple patterns oriented normal to the incident ion beam are observed at intermediate angles of incidence whereas the patterns are rotated by 90° at grazing incidence. For all three materials, the ripple wavelength increases linearly with ion energy what is in agreement with previous observations [24] and indicates that surface-confined ion-enhanced viscous flow dominates the surface smoothing.

Certain differences in the coarsening of the ripple wavelength are observed for the different SiO_2 materials. In the framework of the recent hydrodynamic model of ion erosion [16], these differences are consistent with different surface relaxation rates due to surface-confined ion-enhanced viscous flow and indicate that the surface energies of thermally grown SiO_2 and amorphized quartz are lower and higher than that of fused silica, respectively.

Acknowledgment

We thank R Cuerno for helpful discussions.

References

[1] Chan W L and Chason E 2007 *J. Appl. Phys.* **101** 121301
[2] Makeev M A, Cuerno R and Barabási A-L 2002 *Nucl. Instrum. Methods Phys. Res.* B **197** 185
[3] Chason E, Mayer T M, Kellerman B K, McIlroy D T and Howard A J 1994 *Phys. Rev. Lett.* **72** 3040
[4] Facsko S, Dekorsy T, Trappe C and Kurz H 2000 *Microelectron. Eng.* **53** 245
[5] Mayer T M, Chason E and Howard A J 1994 *J. Appl. Phys.* **76** 1633
[6] Rusponi S, Costantini G, Buatier de Mongeot F, Boragno C and Valbusa U 1999 *Appl. Phys. Lett.* **75** 3318
[7] Toma A, Chiappe D, Šetina Batič B, Godec M, Jenko M and Buatier de Mongeot F 2008 *Phys. Rev.* B **78** 153406

[8] Keller A, Roßbach S, Facsko S and Möller W 2008 *Nanotechnology* **19** 135303
[9] Zhou H, Wang Y, Zhou L, Headrick R L, Özcan A S, Wang Y, Özaydin G, Ludwig K F and Siddons D P 2007 *Phys. Rev.* B **75** 155416
[10] Bradley R M and Harper J M E 1988 *J. Vac. Sci. Technol.* A **6** 2390
[11] Sigmund P 1969 *Phys. Rev.* **184** 383
[12] Sigmund P 1973 *J. Mater. Sci.* **8** 1545
[13] Erlebacher J, Aziz M J, Chason E, Sinclair M B and Floro J A 2000 *J. Vac. Sci. Technol.* A **18** 115
[14] Cuerno R and Barabási A-L 1995 *Phys. Rev. Lett.* **74** 4746
[15] Facsko S, Bobek T, Stahl A, Kurz H and Dekorsy T 2004 *Phys. Rev.* B **69** 153412
[16] Muñoz-García J, Castro M and Cuerno R 2006 *Phys. Rev. Lett.* **96** 086101
[17] Smirnov V K, Kibalov D S, Orlov O M and Graboshnikov V V 2003 *Nanotechnology* **14** 709
[18] Bobek T, Mikuszeit N, Camarero J, Kyrsta S, Yang L, Niño M A, Hofer C, Gridneva L, Arvanitis D, Miranda R, de Miguel J J, Teichert C and Kurz H 2007 *Adv. Mater.* **19** 4375
[19] Oates T W H, Keller A, Facsko S and Mücklich A 2007 *Plasmonics* **2** 47
[20] Toma A, Chiappe D, Massabò D, Boragno C and Buatier de Mongeot F 2008 *Appl. Phys. Lett.* **93** 163104
[21] Bisio F, Moroni R, Buatier de Mongeot F, Canepa M and Mattera L 2006 *Phys. Rev. Lett.* **96** 057204
[22] Liedke M O, Liedke B, Keller A, Hillebrands B, Mücklich A, Facsko S and Fassbender J 2007 *Phys. Rev.* B **75** 220407(R)
[23] Oates T W H, Keller A, Noda S and Facsko S 2008 *Appl. Phys. Lett.* **93** 063106
[24] Umbach C C, Headrick R L and Chang K-C 2001 *Phys. Rev. Lett.* **87** 246104
[25] Toma A, Buatier de Mongeot F, Buzio R, Firpo G, Bhattacharyya S R, Boragno C and Valbusa U 2005 *Nucl. Instrum. Methods. Phys. Res.* B **230** 551
[26] Keller A, Facsko S and Möller W 2009 *Nucl. Instrum. Methods* B **267** 656
[27] Ziegler J F, Biersack J P and Littmark U 1984 *The Stopping and Range of Ions in Solids* (New York: Pergamon)
[28] Davidovitch B, Aziz M J and Brenner M P 2007 *Phys. Rev.* B **76** 205420
[29] Carter G and Vishnyakov V 1996 *Phys. Rev.* B **54** 17647
[30] Mullins W W 1959 *J. Appl. Phys.* **30** 77
[31] Makeev M A and Barabási A-L 1997 *Appl. Phys. Lett.* **71** 2800
[32] Mayr S G and Averback R S 2001 *Phys. Rev. Lett.* **87** 196106
[33] Shchipalov Yu K 2000 *Glass Ceram.* **57** 374
[34] Muñoz-García J, Cuerno R and Castro M 2008 *Phys. Rev.* B **78** 205408
[35] Kardar M, Parisi G and Zhang Y-C 1986 *Phys. Rev. Lett.* **56** 89
[36] Muñoz-García J, Cuerno R and Castro M 2006 *Phys. Rev.* E **74** 050103(R)